12. Sato, N., Hayami, T., Murato, K., Watanabe, K., Kariya, Y., Sakaguchi, M., Kimura, S., Nonada, M. and Kimura, A., *Appl. Microbiol. Biotechnol.*, 1988, **30**, 153–159.
13. Saito, A., Sekino, S., Komatsu, Y., Sato, M., Hirano, T. and Itoh, S., *Gene*, 1988, **73**, 545–552.
14. Koren, Y., Sarid, S., Ber, R. and Daniel, V., *Gene*, 1989, **77**, 309–315.
15. Agellon, A. B. and Chen, T. T., 1989, *DNA*, 1986, **5**, 463–471.
16. Johansen, B., Johansen, O. C. and Valla, S., *Gene*, 1989, **77**, 317–324.
17. Sekine, S., Mizukami, T., Nishi, T., Kuana, Y., Saito, A., Sato, M., Itoh, S. and Kawauchi, H., *Proc. Natl. Acad. Sci. USA*, 1985, **82**, 4306–4310.
18. Villasenor, L. I. G., Zhang, P., Chen, T. T. and Powers, D. A., *Gene*, 1988, **65**, 239–246.
19. Sato, N., Watanabe, K., Murata, K., Sakaguchi, M., Kariya, Y. and Kimura, A., *Biochem. Biophys. Acta*, 1989, **949**, 35–42.
20. Momota, H., Kosugi, R., Ohgai, H., Akihiko, H. and Ishioka, H., *Nucleic Acids Res.*, 1988, **16**, 10362.
21. Peritz, L. N., Fodor, E. J. B., Silversides, D. W., Cattini, P. A., Baxter, J. D. and Ederhardt, N. L., *J. Biol. Chem.*, 1988, **263**, 5005–5007.
22. Gill, J. A., Sumpter, J., Donaldson, E., Dye, H., Souza, L., Berg, T., Wypch, J. and Langley, K., *Biotechnol.*, 1985, **3**, 643-646.
23. Chang, C. N., Rey, M., Bochner, B., Heyneker, H. and Gray, G., *Gene*, 1987, **55**, 189–196.
24. Gary, G., Gerlad, S., Gary, B., Penny, S., Sonia, E., Sylvie, H., Patricia, V. and Charles, J. R., *Gene*, 1984, **32**, 21–30.
25. Nakayama, A., Ando, K., Dawamura, K., Mita, I., Fukuzama, K., Hori, M., Hongo, M. and Furutal, Y., *J. Biotechnol.*, 1988, **8**, 123–134.
26. Pavlakis, G. N., Hizuka, N., Gorden, P., Seeburg, P. and Hamer, D. H., *Proc. Natl. Acad. Sci. USA*, 1981, **78**, 7398–7402.
27. Pasleau, F., Tocci, M. J., Leung, F. and Kopchick, J. J., *Gene*, 1985, **38**, 227–232.
28. Gallardo, A. M., Zavala, M. M., Kelder, B., Taylor, J., Chen, H., Leung, F. C. and Kopchick, J. J., *Gene*, 1988, **70**, 51–56.
29. Pasleau, F., Leung, F. and Kopchick, J. J., *Gene*, 1987, **57**, 47–52.
30. Pavlakis, G. N. and Hamer, D. H., *Proc. Natl. Acad. Sci. USA*, 1983, **80**, 397–401.
31. Wagner, E. F., *EMBO J.*, 1990, **9**, 3025–3032.
32. Klein, T. M., Aventeen, R., Lewis, P. A. and McElligo, H. S. F., *Biotechnology*, 1992, **10**, 286–291.
33. Vize, P. D., Michalska, A. E., Ashman, R., Llyod, B., Stone, B. A., Quinn, F., Wells, J. R. E. and Seamark, R. F., *J. Cell Sci.*, 1988, **90**, 295–300.
34. Zhu, Z., Xu, K., Li, G., Xie, Y. and He, L., *Kexue Tongbao Academia Sinica*, 1986, **31**, 988–990.
35. Chourrout, D., Guyomard, R. and Houdebine, L., *Aquaculture*, 1986, **51**, 143–150.
36. Zhu, Z., Li, G., He, L. and Chen, S., *A. Angen Ichthyol.*, 1985, **1**, 32–34.
37. Guyomard, R., Chourrout, D. and Houdebine, L., *UCLA Symp. Mol. Cell Biol. New Series*, 1988, **87**, 10–19.
38. Liu, Z., Moav, B., Faras, A. J., Guise, K. S., Kapuscinski, A. R. and Hackett, P. B., *Biotechnology*, 1990, **8**, 1268–1272.
39. Do, S. J., Gong, Z., Fletcher, G. L., Shears, M. A., King, M. J., Idler, D. R. and Hew, C. L., *Biotechnol.*, 1992, **10**, 176–181.
40. Pandian, T. J., Kavumpurath, S., Mathavan, S. and Dharmalingam, K., *Curr. Sci.*, 1992, **60**, 596–600.
41. Stuart, G. W., McMurray, J. V. and Westerfield, M., *Development*, 1988, **103**, 403–412.

Received 13 July 1992; accepted 30 July 1992

RESEARCH ARTICLE

Adequacy of thermosyphon cooling for an Indian PHWR

P. K. Vijayan, V. Venkat Raj, D. S. Pilkhwal and S. K. Mehta*

Reactor Safety Division, *Reactor Group, Bhabha Atomic Research Centre, Trombay, Bombay 400 085, India

The phenomenon of thermosyphon plays an important role in core heat removal in Indian pressurized heavy water reactors (PHWRs) following failure of primary coolant circulating pumps. To confirm the adequacy of thermosyphon cooling, tests were carried out on the first unit of Narora Atomic Power Station. This was the first time such a test was done in an Indian nuclear power reactor, even though such tests are carried out routinely in many countries. These tests were carried out during the commissioning of the reactor at power levels corresponding to decay heat following reactor shutdown. We describe here the thermosyphon tests conducted, the results obtained and the analysis of the data generated.

NUCLEAR reactors are designed for safety not only under normal operating conditions but also under off-normal and accident conditions. One such off-normal condition is the complete loss of coolant pumping power. Under this condition even though the reactor shuts down, the heat generated by decay of fission products needs to be removed to maintain fuel temperatures within safe limits. This is effected by coastdown of the circulating

flow initially, followed by thermosyphon flow of the primary coolant. The phenomenon of thermosyphon cooling in nuclear reactors assumes significance since this is a completely passive mode of core cooling without the aid of any fluid moving machinery and can be relied upon to remove decay heat in the event of a total power failure.

The present article is devoted to the investigations on thermosyphon cooling in the primary coolant loop of a pressurized heavy water reactor (PHWR). Figure 1 shows a simplified flow diagram of the primary heat transport (PHT) system of a PHWR. The primary heat transport loop comprises of two passes of the coolant past the fuel. Thus the coolant passes through half-core 1, steam generator 1, pump 1, half-core 2, steam generator 2, pump 2 and back to half-core 1. This path of the coolant shown by arrows in Figure 1 is known as a figure-of-eight loop. In a 220 MWe PHWR, each core pass includes 153 horizontal fuel channels located at different elevations inside the calandria vessel as shown in Figure 2. Each channel is connected by an inlet and an outlet feeder to large diameter (400 mm) inlet and outlet headers. Large diameter piping (400 mm) connects the headers to the steam generators (SGs) and pumps. Two steam generators and two pumps are connected in parallel between a reactor outlet header (ROH) and a

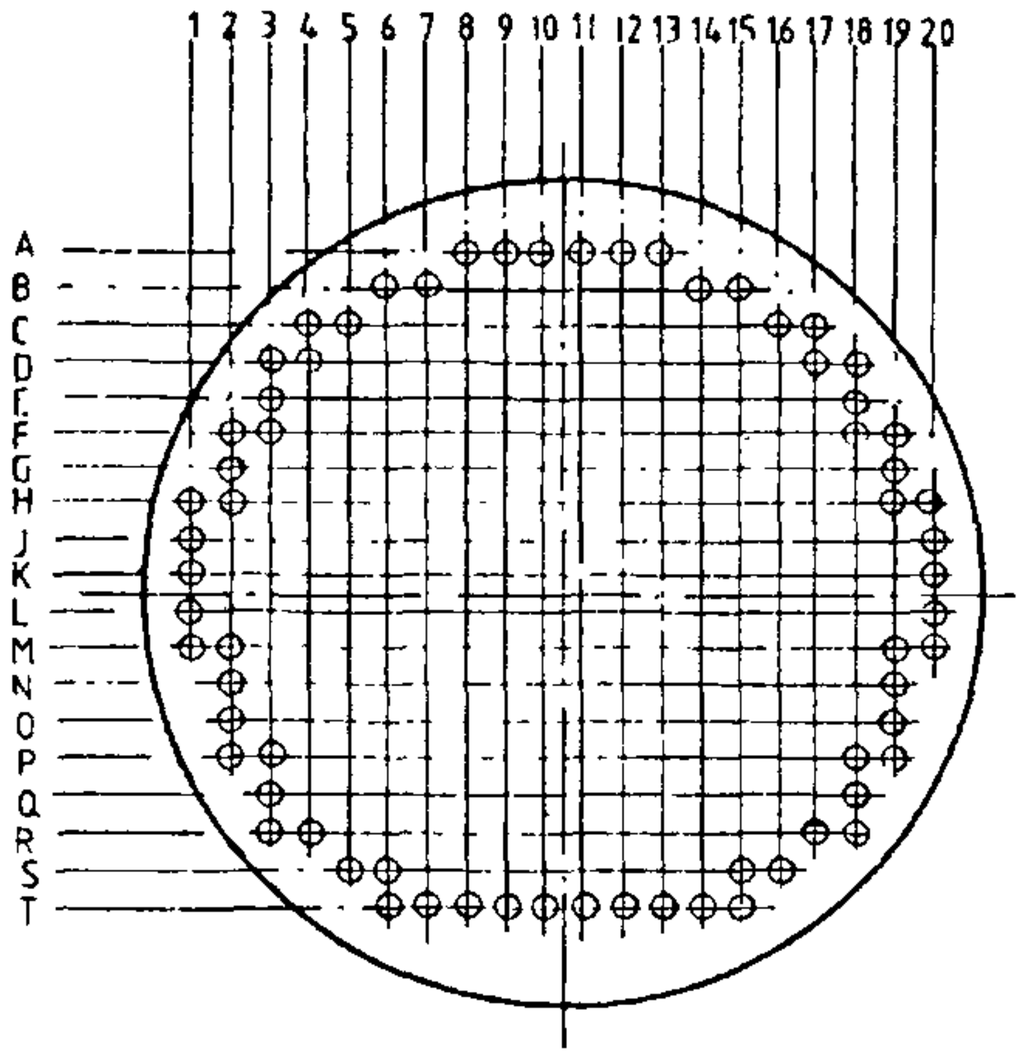

Figure 2. Channel layout in calandria for 220 MWe PHWR.

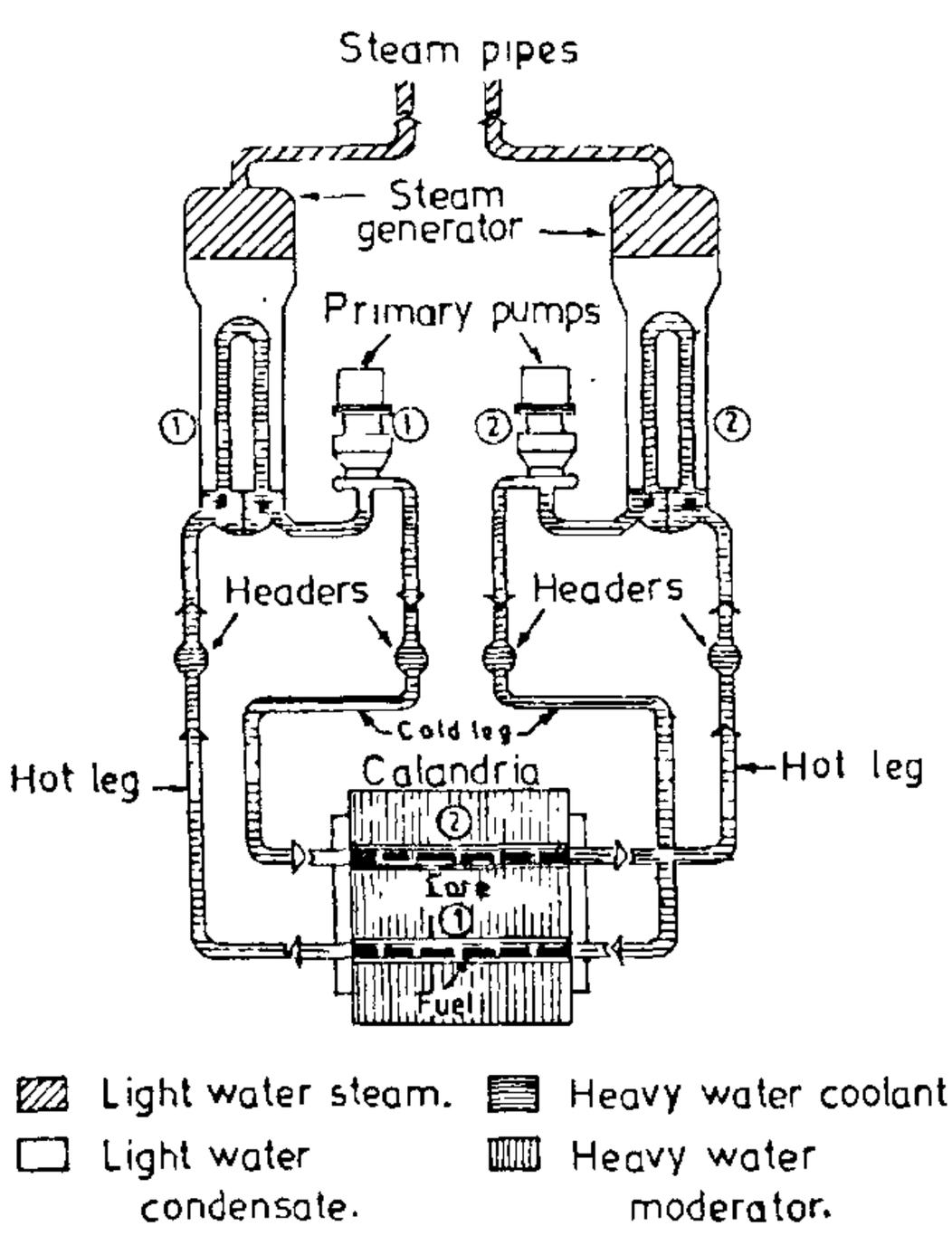

Figure 1. Simplified flow diagram of the primary heat transport system of a PHWR.

reactor inlet header (RIH). The SGs comprise of a shell in which are housed a large number of vertical inverted U-tubes through which the hot heavy water flows. The secondary side of the steam generator has light water as coolant with its flow maintained by natural circulation. The top of the SG U-tubes is about 16 m above the headers and the headers are located about 7 m above the core centre line. The total elevation difference between the centre of the core and the top of the U-tubes is about 23 m. The density difference in this height provides the buoyancy force for thermosyphoning.

To understand the thermosyphon behaviour of the primary coolant loop with horizontal fuel channels, phenomenological studies were carried out in a simple figure-of-eight loop[1-5]. Based on the results of these experimental studies, a computer code TINFLO-III[6,7] was developed for the analysis of thermosyphon behaviour in PHWRs. This computer code was extensively used for predicting thermosyphon behaviour in 220 MWe and 500 MWe PHWRs[8]. With a view to verifying the code predictions and also to demonstrate, in-plant, the onset of thermosyphon cooling, tests were carried out in one of the reactors at the Narora Atomic Power Station (NAPS). The various safety issues were examined and a suitable test procedure was evolved. Approval of the safety and regulatory authorities was obtained. As per the approved procedure, thermosyphon tests were conducted in Unit 1 of NAPS.

Tests conducted

Three thermosyphon tests were conducted in Unit 1 of

Narora Atomic Power Station, with the reactor critical at power levels of 0.956, 1.991 and 3.249 per cent of full power (FP). The initial conditions for the tests which were conducted during the commissioning of the reactor are described below.

For all the tests, the water level in the secondary side of the SG was maintained at the normal operating value whereas its pressure was lowered to obtain a saturation temperature of about 200° C. On the primary side, the pressure was maintained same as that at normal operating conditions. The initial conditions of flow and temperature on the primary side were somewhat different for the three tests. For the 0.956% FP and 1.991% FP tests, two PHT system pumps were running (1–1 mode of pump operation). Since the boiler branches with the idle pumps were isolated, the heat removal was accomplished by only two SGs in the 0.956% FP test. For the 1.991% FP test, on the other hand, the boiler branches having idle pumps were not isolated and heat removal was by all the four SGs. The flow in the SGs on the idle pump branches was in the reverse direction to start with. For the test at 3.249% FP, the initial PHT system flow rate, pressure and temperature corresponded to those of steady state thermosyphon at 1.991% FP (the PHT system pumps remaining in the switched off condition).

Tests at 0.956% and 1.991% FP were initiated by switching off the PHT system pumps. The test at 3.249% FP was initiated by increasing the power from 1.991% FP to 3.249% FP when the reactor was thermosyphoning at 1.991% FP.

The important parameters recorded during the tests are

- Channel flows and temperature differences (ΔT) for 16 fuel channels
- SG ΔT, pressure and level for all the four SGs
- pressure drop (ΔP) across the RIH and the corresponding ROH
- PHT system pressure
- Neutron power and
- Channel outlet temperatures for all the channels.

In addition, other operational parameters were also recorded.

Test results

Transient behaviour

The observed transient behaviour for the tests at different powers is similar. Hence typical transient results obtained from the 0.956% FP test only are presented here. A complete description of the test results are given in refs. 9, 10.

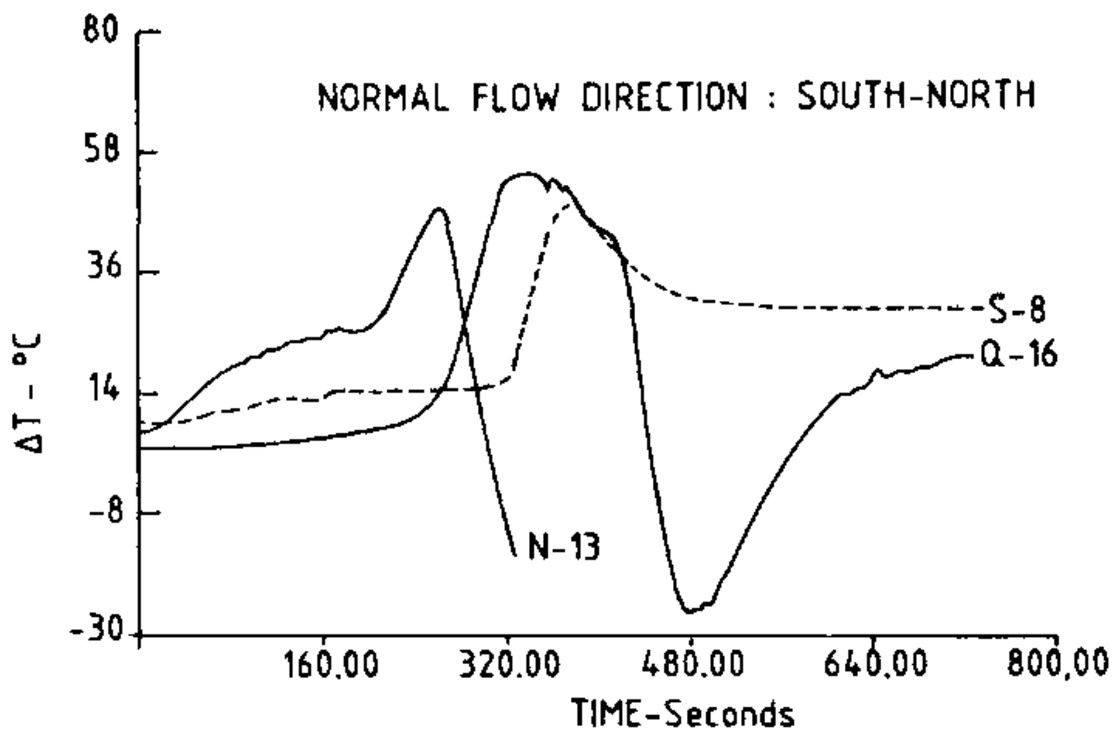

Figure 3. Channel ΔT variation for test at 0.956% FP.

The channel ΔT transients are plotted in Figure 3. Typical transient variation representative of most of the channels is shown by channel S-8. The ΔT reaches a peak value before the steady state is reached. The peak and the steady state values for most of the channels are quite close to each other, although their time of occurrences vary.

The transient behaviour of ΔT for channels N-13 and Q-16, shown in Figure 3, needs special mention. In channel N-13, the ΔT increased as expected up to a time of about 265 sec and then suddenly started reducing at a very fast rate and went out of the chart range of the recorder at about 325 sec. Just before going out of the chart range, the ΔT indication was about $-16.1°$ C, i.e. 16.1° C ΔT with flow reversal. The ΔT variation of channel Q-16, on the other hand, shows a peak ($\approx 54.7°$ C) at about 340 sec and then suddenly reduces and then goes to about $-25.7°$ C (with flow reversal) at about 480 sec. Subsequently, the ΔT increases and the flow direction changes again to the original and the ΔT stabilizes at about 21.4° C. Thus flow reversal has taken place twice in this channel and hence the initial and final steady state flow directions in the channel are the same leading to positive ΔT before and after the flow reversals. Channel flow reversals, during transient thermosyphoning, have been reported for CANDU systems[11] as well as for flow in SG tubes during thermosyphoning[12]. None of the monitored channel ΔTs showed negative values for the 1.991% and 3.249% FP tests indicating the absence of flow reversal.

Steady state behaviour

The gross thermosyphon flows at different powers were estimated by the heat balance method using the measured ΔT across the steam generator and the

measured neutron power. These are presented in Table 1. The flow rates so estimated are seen to increase with power as expected.

Channel temperature monitoring (CTM) system data

The measurements obtained from the CTM system give the individual channel outlet temperatures. Since the channels at the bottom of the calandria have a larger elevation difference compared to the top channels, the flows in the lower channels are expected to be more than those in the top channels. This would indicate lower channel outlet temperatures for the bottom channels compared to the corresponding top channels generating the same power. This trend is generally observed for the tests at 1.991% and 3.249% FP. The data for 0.956% FP test, however, do not show the same trend. This is attributed to the isolation of the two SGs and the flow reversals observed in some channels.

Method

Analysis for test conditions was carried out using the computer code TINFLO-III, which solves the one-dimensional momentum and energy equations using the finite difference method. Flow coastdown phase is modelled based on the test data on pump speed versus time. Steam generator secondary side is modelled by a single volume. Initial temperature on the SG secondary side is specified as input and the primary temperatures are calculated by the code. The code lumps all parallel flow paths in the half core into one equivalent flow path. Therefore the code can predict only the average core behaviour and not the individual channel behaviour. Further details of the code and the solution procedure are given in ref. 7.

Results

Since the predicted transients are similar for the tests at different powers, the results are presented for the test at 0.956% FP only. A complete description of the predicted transient behaviour is given in ref. 13. The observed and predicted transient behaviour of some of the important parameters are compared and discussed in the following sections.

Table 1. Estimated steady state thermosyphon flow rate

Power (%)	Measured SG ΔT (°C)	Estimated flow (%)
0.956	34 7	1.3
1 991	41 0	2.3
3 249	60 9	2 5

Header to header pressure drop

Figure 4 shows the measured and predicted variation of header to header pressure drop for the test at 0.956% FP. The prediction and the measurements show the same trend. However, the test data show small amplitude oscillations, which are not seen in the predictions. Also, there is a time lag between the predicted and measured minimum and maximum pressure drops. At time $t=0$, and ΔP indications are off-scale since these ΔP indicators have a range of only -250 cm to $+250$ cm and ΔP is much higher than this (≈ 13000 cm) when the primary pumps are operating. The first indication of header ΔP is obtained at about 40 sec after the pumps are switched off.

Channel ΔT variation

Figure 5 shows the measured (average) and predicted channel ΔT variations for the test at 0.956% FP. The experimental curve is the mean of the seven channel ΔTs recorded by the control room computer. The measured and predicted ΔTs show the same trend. Although the agreement between the measured and predicted steady state value is quite good, the predicted peak value is much larger (about 30%) than that measured. The experimental peak value is observed to be lower than the predicted peak due to the following reasons. The different channels have different feeder lengths and are located at different elevations and therefore individual peaks having different values occur at different times. Hence, on averaging the ΔTs, a smaller peak value is obtained. However, in the analysis all the channels in one half core are lumped into one

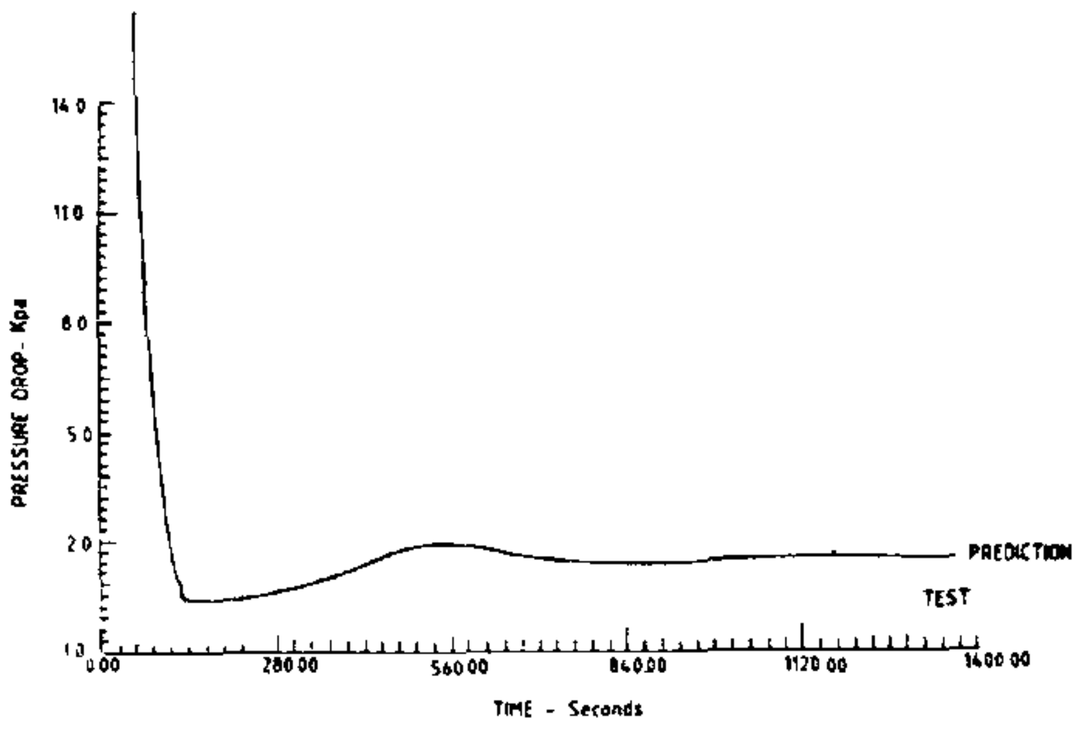

Figure 4. Variation of header to header pressure drop for test at 0 956% FP.

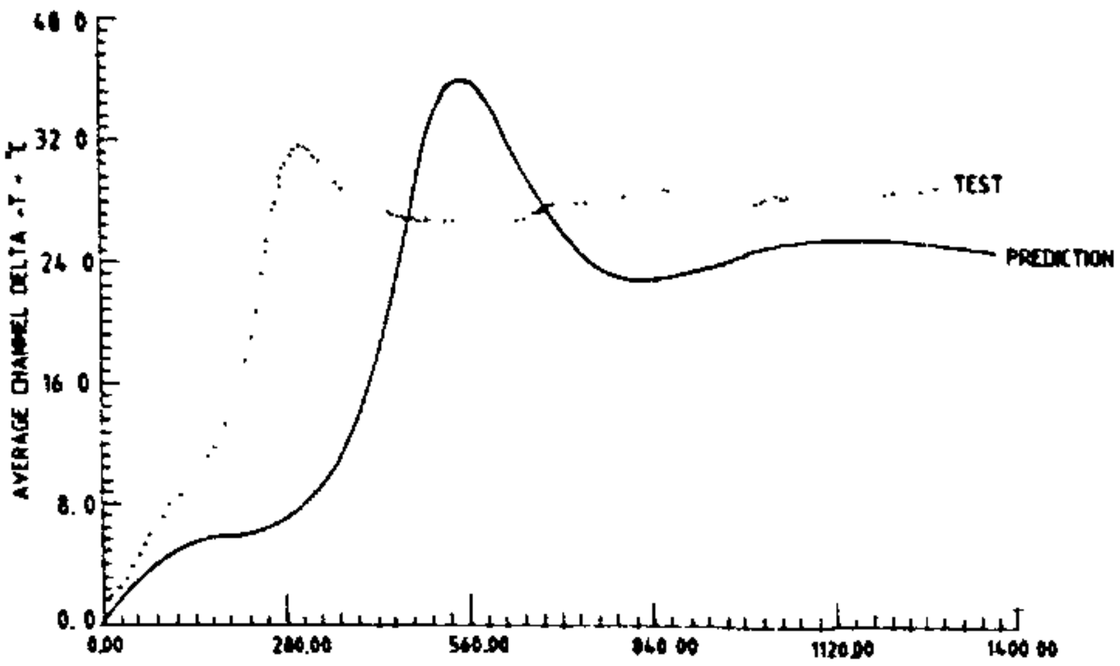

Figure 5. Variation of average channel ΔT for test at 0.956% FP.

equivalent channel having one length and one elevation. Lumping also leads to a time lag between the peak values predicted and obtained during the tests. Improvement of prediction with regard to this aspect can be obtained by avoiding the lumping of all the parallel channels in a half core. However, this will involve increase in computational effort.

Steam generator ΔT variation

Figure 6 shows the steam generator ΔT variations predicted and measured during the test at 0·956% FP. Again, the general trend is well predicted by the code. As in the case of channel ΔT transient, the predicted peak values are found to be about 30% higher than the experimental value. This is attributed to the lumping of the parallel channels in the core and the steam generator. All the SG U-tubes are assumed to be of the same length in the calculation. This introduces a time lag which will be added to that observed due to the differences in channel length.

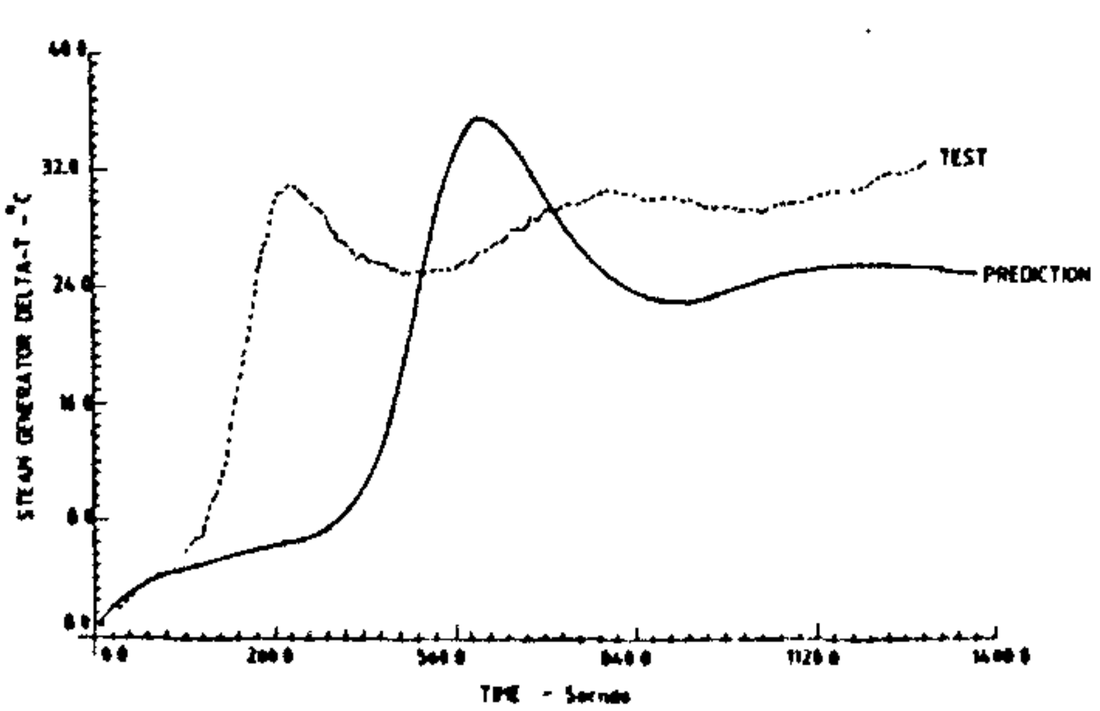

Figure 6. Variation of steam generator ΔT with time for test at 0·956% FP.

Steady state behaviour

The steady state flow rate for the test condition was estimated by the heat balance method using the measured core power and ΔT across the steam generators. This is compared with the steady state core flow predicted by TINFLO-III in Figure 7. The measured and predicted steady state header to header ΔP is also compared in this figure. Except for the test at 0.956% FP, the steady state parameters are seen to be predicted within about $\pm 20\%$ of the test values by TINFLO-III. For the 0.956% FP test, flow reversal was observed in some channels. In the event of a flow reversal, heat balance will not give the proper loop flow rate. The large percentage deviation between the measured and predicted steady state values for the test at 0.956% FP is attributed to this fact.

Conclusions

The thermosyphon tests conducted in Unit-1 of NAPS have confirmed the adequacy of thermosyphon cooling at decay power levels following failure of forced circulation of the primary coolant. This is an important design feature which enhances the safety of the reactor under such off-normal conditions. The channel elevation plays a significant role in determining the flow rate through the different channels during thermosyphoning. Analysis has been carried out for the test conditions, using the computer code TINFLO-III. In general, the predictions and the test data show similar trends. The magnitudes of the steady state values of various parameters are generally predicted within about $\pm 20\%$

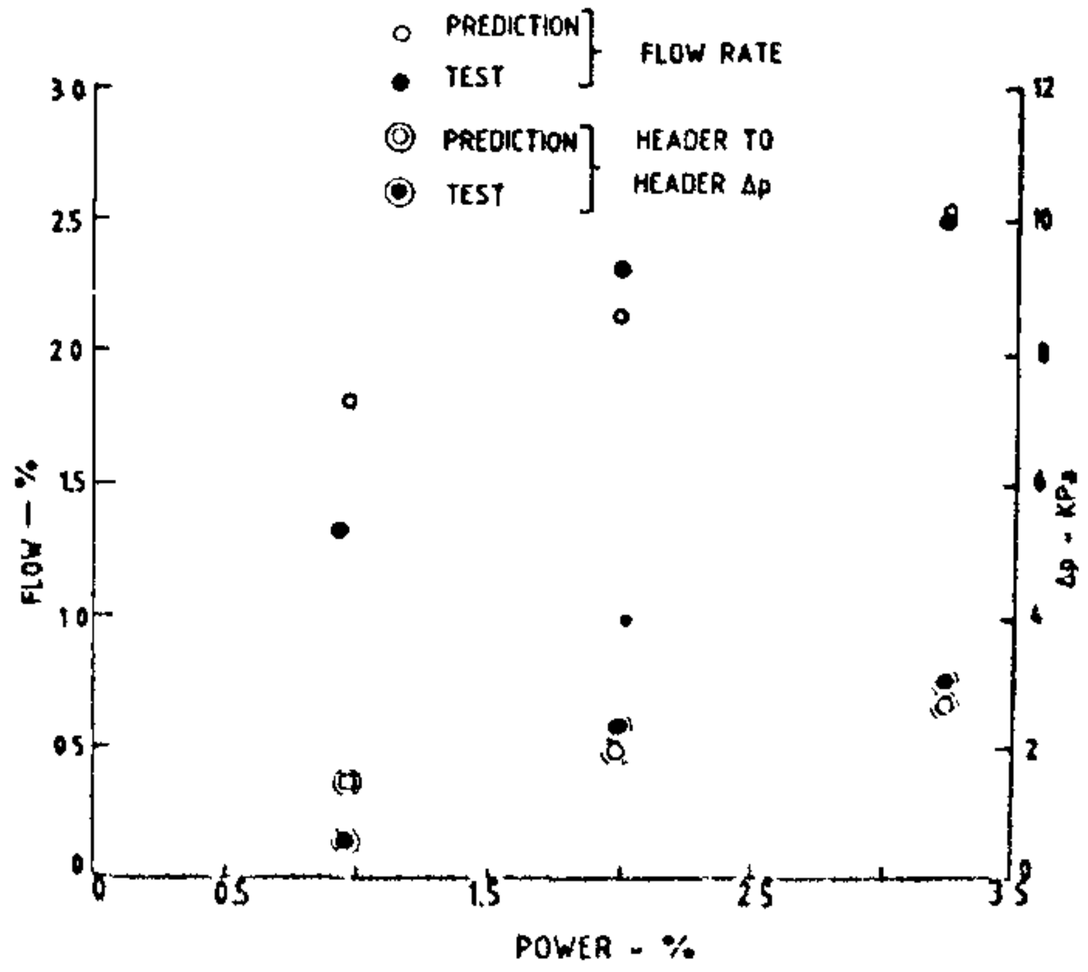

Figure 7. Measured and predicted steady state flow rate and header to header ΔP.

of the test data. The peak values of channel and SG ΔTs are predicted within about $\pm 30\%$ of the test data.

1 Vijayan, P. K., Ph D thesis, IIT, Bombay, 1988.
2. Vijayan, P. K., Venkat Raj, V., Mehta, S. K. and Date, A. W., 85-WA HT-17, Paper published at the Winter Annual Meeting of ASME, Miami Beach, Florida, November 17–21, 1985.
3. Vijayan, P. K. and Date, A. W., *Int. J. Heat Mass Transfer*, 1990, 33, 2479–2489.
4 Vijayan, P. K., Mehta, S. K. and Date, A. W., *Int. J. Heat Mass Transfer*, 1991, 34, 2219–2230.
5 Vijayan, P. K. and Date, A. W., *Nucl. Eng. Des.*, 1992, (to appear).
6. Vijayan, P. K., Nagdaune, R. K. and Venkat Raj, V., Paper presented at the National Systems Conference, Regional Engg. College, Kurukshetra, India, 1987.
7. Vijayan, P. K., Nagdaune, R. K. and Venkat Raj, V., Proceedings of the Indo-Polish Seminar on Development of Advanced Codes and Methods for Transient and Accident Analysis of Nuclear Power Plants, Bombay, 1988, pp. 10 1–10 26.
8. Nagdaune, R. K., Vijayan, P. K. and Venkat Raj, V., Report No. 005/DEV/05011–2 (PO), November 1987.
9. Vijayan, P. K., Venkat Raj, V. and Pilkhwal, D. S., Thermosyphon Tests conducted on unit 1 of Narora Atomic Power Station, BARC Report under publication.
10. Vijayan, P. K., Venkat Raj, V. and Mehta, S. K., Proceedings of the 11th National Heat and Mass Transfer Conference, December 21–23, 1991, Madras, India.
11. Caplan, M. Z., Gulshani, P., Holmes, R. W. and Wright, A. C. D., Proceedings of Specialists' Meeting organized by the IAEA, Budapest, Hungary, 1983.
12. Kukita, Y., Nakamura, H., Tasaka, K. and Chauliac, C., *Nucl. Sci. Eng.*, 1985, **99**, 289–298.
13. Vijayan, P. K., Venkat Raj, V., Nagdaune, R. K. and Pilkhwal, D. S., Third International Symposium on Small and Medium Sized Nuclear Reactors, August 21–23, 1991, New Delhi, India.

Received 23 October 1992; accepted 31 October 1992

RESEARCH COMMUNICATIONS

Pore size dependence on doping concentration in porous silicon

R. M. Vadjikar and R. V. Nandedkar
Centre for Advanced Technology, Indore 452 013, India

The dependence of pore size on doping concentration in porous silicon layers is reported here. Porous silicon layers were fabricated on $N^+/N/N^+$-doped silicon wafers by electrochemical etching at current density of 40 mA/cm^2 for 50 min, under ambient light conditions. Scanning electron microscopy results show that pore sizes change as the doping concentration changes in the silicon wafer. These results are discussed in view of the pore formation mechanism.

THE fabrication of porous silicon layers by electrochemical dissolution of single crystal silicon has been known since 1956[1]. The high reactivity and large surface area of porous silicon layers has spurred further investigations for several applications. The capability of easily forming an oxide layer on porous silicon has been utilized for electronic isolation in semiconductor fabrication processes such as silicon-on-insulator (SOI) and fully isolated porous oxidized silicon (FIPOS)[2,3]. Thick and stress-free silicon nitride/oxynitride films have been produced from porous silicon[4]. Fabrication of conducting tungsten films and silicon carbide layers is under investigation[5,6]. Surface micromachining of silicon has been reported by using porous silicon as a sacrificial layer[7]. The highly reactive nature of porous silicon has been used for chemical sensors applications[8].

In spite of the considerable interest in porous silicon, its basic formation mechanism and material properties are still not well-established. Theunissen[9] proposed that the origin of etch channels is because of local breakdown of electric field barrier at the surface of silicon. The precise location of such a breakdown is dependent on crystal defects, impurities, fluctuations in dopant concentration and electrochemical dissolution conditions. Beale *et al.*[10] have extended this model and explained the formation of porous silicon films by suggesting that the Fermi level of silicon in porous silicon is pinned near the mid-gap. This causes the silicon–electrolyte system to behave like a Schottky barrier diode. The current flow through the Schottky barrier, by tunneling or thermionic emission, causes silicon dissolution at some locations. Once the pores are initiated at such locations, their propagation is explained by preferential current flow through the lower resistivity electrolyte rather than through fully depleted porous silicon. The Beale model does not explain all aspects of porous silicon formation[11]. More recently, Smith *et al.*[11] have proposed a diffusion-limited model. This model explains pore formation by availability of diffusion-controlled electrons/holes at the silicon–electrolyte interface. Lehmann and Gosele[12] have proposed a quantum confinement model for porous silicon formation. They suggest that the bandgap in porous silicon increases due to quantum charge confinement within the small dimensions of silicon wires formed in porous silicon. The increased bandgap leads to charge depletion which limits further dissolution of silicon wires. The dependence of pore morphology on the doping concentration and type has been reported by several investigators[9,13,14]. Electro-